Measurement of $\chi^{(3)}$ for Doubly Vibrationally Enhanced Four Wave Mixing Spectroscopy

Wei Zhao and John C. Wright
Department of Chemistry, University of Wisconsin, Madison, Wisconsin 53706
(Received 26 April 1999)

We report the measurement of the third order susceptibility $\chi^{(3)}$ for doubly vibrationally enhanced four wave mixing in the model system, acetonitrile. Two resonances multiplicatively increase the mixing efficiency if there is mode coupling and provide an additional spectral dimension for vibrational spectroscopy that greatly improves its resolution. Such methods promise to have important applications for vibrational spectroscopy of complex materials.

PACS numbers: 42.65.An, 33.20.Ea, 33.80.–b

Vibrational spectroscopy is widely used for studying materials because it provides molecular level characterization. Its use is often hindered in complex materials because spectral congestion and line broadening obscure transitions. There is great interest in developing multiresonant six wave mixing (SWM) spectroscopies that can increase selectivity [1–7]. A different approach uses multiresonant four wave mixing (FWM) and indeed, selective enhancements and line narrowing have been demonstrated with FWM for electronic transitions at cryogenic temperatures [8]. In this paper, we extend FWM to vibrational resonances and report the first measurement of the multiplicative vibrational enhancement of $\chi^{(3)}$. The measurement of a doubly vibrationally enhanced (DOVE) $\chi^{(3)}$ shows the feasibility for multidimensional vibrational spectroscopies.

There are many nonlinear processes that must be considered [3]. Figure 1 shows the important nonlinear processes for this work. In the DOVE-IRFWM process [Fig. 1(a)], coherent sources drive the acetonitrile (CH_3CN) absorptions near the ν_2 C≡N stretch at $\omega_2 = 2253\ \mathrm{cm}^{-1}$ and the $\nu_2 + \nu_4$ (C≡N + C—C stretch) combination band at $\omega_1 = 3164\ \mathrm{cm}^{-1}$. A third beam at 532 nm generates the output coherence by a two photon Raman process that destroys the ν_4 excitation. The Mukamel diagram in Fig. 1(a) shows how the bra and ket parts of the coherence $\rho_{i,j}$ evolve along three different time ordered pathways [9]. Each pathway can be resonantly enhanced (see Fig. 1) and described quantitatively by [3]

$$\rho_{db} = \left(\frac{\Omega_{ac}\Omega_{ab}\Omega_{cd}}{\Delta_{ca}\Delta_{da}\Delta_{db}} + \frac{\Omega_{ac}\Omega_{ab}\Omega_{cd}}{\Delta_{ca}\Delta_{cb}\Delta_{db}} + \frac{\Omega_{ac}\Omega_{ab}\Omega_{cd}}{\Delta_{ab}\Delta_{cb}\Delta_{db}}\right)\rho_{aa}\,, \tag{1}$$

where each term corresponds to a pathway. Here, Ω_{ij} is the Rabi frequency, $\mu_{ij}E/2\hbar$, of the transition between states i and j, μ_{ij} is the transition moment, E is the resonant laser field, $\Delta_{ij} \equiv \omega_{ij} - \omega_k - i\Gamma_{ij}$, ω_{ij} is the frequency difference between states i and j, ω_k is the laser frequency, and Γ_{ij} is the dephasing rate. This equation can be rewritten in the form

$$\rho_{db} = \frac{\Omega_{ac}\Omega_{ab}\Omega_{cd}}{\Delta^*_{ba}\Delta_{ca}}\left(\frac{1}{\Delta_{da}} + \frac{i\Gamma^a_{db}}{\Delta_{da}\Delta_{db}} + \frac{i\Gamma^a_{cb}}{\Delta_{cb}\Delta_{db}}\right)\rho_{aa}\,, \tag{2}$$

where $\Gamma^a_{ij} = \Gamma^*_{ij} - \Gamma^*_{ia} - \Gamma^*_{aj} - \Gamma_{aa}$ and Γ^*_{ij} is the pure dephasing rate of the ij transition. The last two terms vanish in the limit of no pure dephasing [3]. The second FWM process is shown in Fig. 1(b). If state c is an electronic state, this process is coherent anti-Stokes Raman spectroscopy (CARS) [9] but if state c is a vibrational state, it is a DOVE Raman process given by [3]

$$\rho_{da} = \frac{\Omega_{ac}\Omega_{cb}\Omega_{bd}}{\Delta_{ca}\Delta_{ba}\Delta_{da}}\rho_{aa}\,. \tag{3}$$

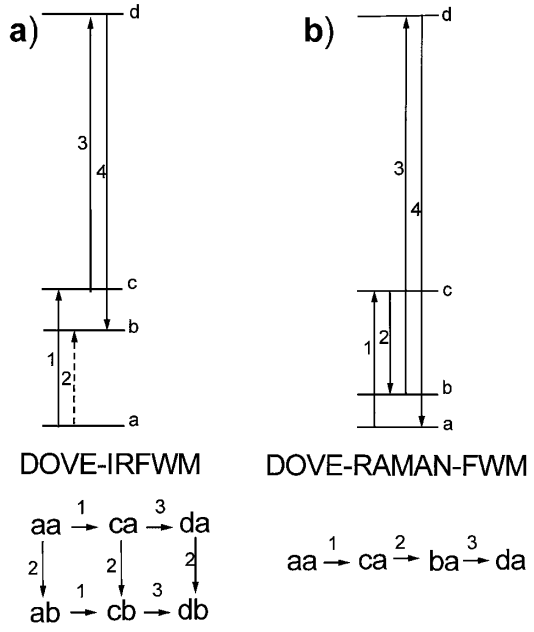

FIG. 1. The resonances for DOVE with three input frequencies (ω_1, ω_2, ω_3) and the output signal (ω_4). The horizontal lines indicate resonant vibrational or nonresonant electronic states. The solid and dotted vertical arrows indicate resonances associated with the ket or bra part of the coherence. The letters in the bottom Mukamel diagrams represent state changes in the ij of the ρ_{ij} density matrix.

 0031-9007/99/83(10)/1950(4)$15.00

The DOVE signals require mode coupling between the resonant vibrational modes since at least one of the transition moments in the numerator must involve changes in both vibrational quanta [7,10,11]. The changes are the same as those responsible for combination bands that occur in one or more of the infrared or Raman transitions.

In the Maker-Terhune convention, the third order susceptibility for the DOVE-IRFWM and CARS processes are

$$\chi_D^{(3)} = \frac{NF\mu_{ac}\mu_{ab}\mu_{cd}\mu_{db}}{4D\hbar^3\Delta_{ca}\Delta_{ba}^*\Delta_{da}}\rho_{aa}, \quad (4)$$

$$\chi_R^{(3)} = \frac{NF\mu_{ac}\mu_{cb}\mu_{bd}\mu_{da}}{4D\hbar^3\Delta_{ca}\Delta_{ba}\Delta_{da}}\rho_{aa}, \quad (5)$$

where N is the concentration of a component, F is the local field correction, and D accounts for different permutations in defining χ [9]. The macroscopic $\chi^{(3)}$ are directly related to the microscopic hyperpolarizabilities γ by $\chi^{(3)} = NF\gamma$. In order to measure $\chi_D^{(3)}$, we adapted the FWM interferometric method of Levenson and Bloembergen [12] using the 944 cm^{-1} mode of deuterobenzene as an internal standard. Detailed fitting of the line shapes provides a direct way to compare $\chi^{(3)}$ values and avoids measuring absolute intensities. The $\chi^{(3)}$ for the sample is

$$\chi^{(3)} = \sum_{\substack{i=\text{all components}\\ b,c=\text{all states}}} N_i A_i e^{i\theta} i + \frac{N_i B_{ba}^i}{\omega_{ba} - \omega_1 + \omega_2 - i\Gamma_{ba}} + \frac{N_i C_{cb}^i}{(\omega_{ca} - \omega_1 - i\Gamma_{ca})(\omega_{ba} - \omega_2 + i\Gamma_{ba})} + \frac{N_i D_{cb}^i}{(\omega_{ca} - \omega_1 - i\Gamma_{ca})(\omega_{ba} - \omega_1 + \omega_2 - i\Gamma_{ba})}, \quad (6)$$

where N_i represents the component concentrations and the A, B, C, and D contain the transition moments, electronic detuning factors, and local field corrections that describe the amplitudes of nonresonant electronic, Raman, DOVE-IRFWM, and DOVE-Raman contributions, respectively. We do not include electronic resonances, pure dephasing, or singly vibrationally enhanced (SIVE) processes in $\chi^{(3)}$ [13] because we do not see measurable contributions in these spectra. Since the FWM intensity is proportional to $|\chi^{(3)}|^2$, there are cross terms that control the line shapes and allow direct comparisons between the acetonitrile and the deuterobenzene internal standard.

The DOVE-IRFWM was performed by focusing the ω_1, ω_2, and ω_3 beams into the sample. The ω_1 and ω_3 beams were collinear while the ω_2 beam was angled at 13° to optimize the phase matching. The sample cell was a rectangular 100 μm thick glass capillary. The experiments were performed at a constant value of ω_2 while scanning ω_1 across the region of the combination band and monitoring the intensity of the $\omega_4 = \omega_1 - \omega_2 + \omega_3$ output. This approach avoids the problems with the absorption path length and refractive index changes that perturb the four wave mixing if ω_2 is scanned in the region of the strong C≡N absorption. Least squares fitting to Eq. (6) allowed determination of the nonlinear parameters. The model was corrected for the refractive index dispersion and absorption using the data of Bertie [14].

Figure 2 shows a series of FWM spectra obtained for different values of ω_2 and deuterobenzene concentrations. In order to record a sample spectrum without any DOVE contributions, ω_2 was tuned to 2500 cm^{-1}, a value that is far from any vibrational resonance. The only features that appear [see Fig. 2(a)] are the acetonitrile $\omega_1 - \omega_2 = 918$ and deuterobenzene 944 cm^{-1} Raman lines. The deuterobenzene concentration is only 3 mole % in order to make the much stronger 944 cm^{-1} Raman line comparable to the 918 cm^{-1} line. If ω_2 in Fig. 2(b) is tuned to the C≡N stretch at 2253 cm^{-1}, an intense new DOVE-IRFWM line develops at $\omega_1 = 3164$ cm^{-1}, the $\nu_2 + \nu_4$ combination band position. The 944 cm^{-1} Raman line is now a weak feature and the 918 cm^{-1} Raman line is a very weak feature on the shoulder of the DOVE-IRFWM line. In order to observe comparable intensity for the 944 cm^{-1} line, the deuterobenzene concentration must be raised. The spectra for samples with 9 and 29 mole % deuterobenzene are shown in Figs. 2(c) and 2(d). The 944 cm^{-1} Raman line grows quadratically in intensity for higher deuterobenzene concentrations until it becomes comparable with the DOVE-IRFWM line. The Raman line position changes on the ω_1 axis for different positions of ω_2 such that $\omega_1 - \omega_2$ is a constant. The DOVE-IRFWM

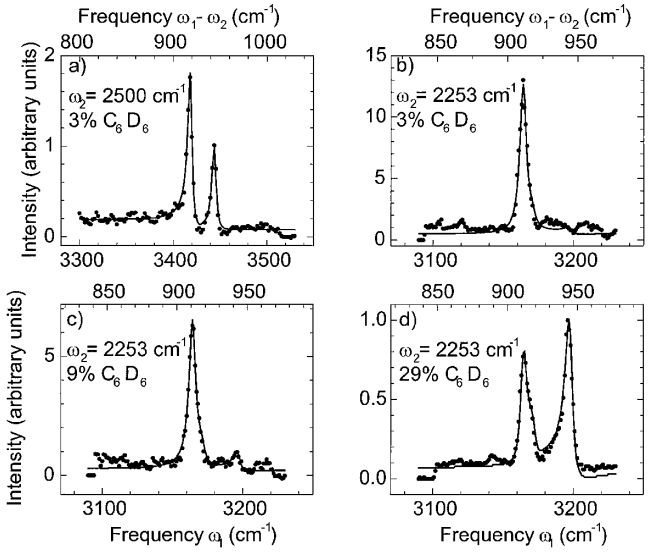

FIG. 2. Four wave mixing scans of ω_1 where ω_2 and the C_6D_6 concentrations are indicated in the figure.

position remains at the same value of ω_1, but its intensity decreases sharply when $\omega_2 \neq 2253$ cm^{-1} confirming the double resonance multiplicative enhancement.

Spectra were also taken by scanning ω_1 in other spectral regions with ω_2 set for the C≡N stretch mode. In particular, we did not observe any DOVE features near the acetonitrile C—H stretch modes, despite their strong infrared and Raman transitions. Their absence reflects an important feature of DOVE methods—lines that lack mode coupling are not seen. In this case, there is no mode coupling between the C≡N and C—H modes that allows double resonances. It is expected that the selectivity imposed by the mode coupling requirement is important for applications because it can reduce spectral congestion in complex samples. We did observe weaker features including a DOVE-Raman cross peak involving ν_4 and the $\nu_3 + 2\nu_4$ combination band and a DOVE-IRFWM cross peak involving the $\nu_3 + \nu_4$ and $\nu_3 + 2\nu_4$ combination bands.

Since the $\omega_2 = 2500$ cm^{-1} spectrum does not contain contributions from DOVE resonances, it can be fitted using the known deuterobenzene Raman and nonresonant electronic $\chi^{(3)}$ [12] to obtain the acetonitrile Raman and nonresonant electronic $\chi^{(3)}$ as well as the windows nonresonant $\chi^{(3)}$. These values can then be used to fit the remaining spectra. The transition linewidths and positions were calculated directly from the spectra and the DOVE $\chi^{(3)}$ values were adjusted to fit each spectrum. The theoretical results are shown as the solid lines in Fig. 2 and the important parameters are summarized in Table I. The DOVE $\chi^{(3)}$ values use the 29% sample data where the comparison is most accurate. The DOVE-IRFWM linewidth is significantly narrower than the absorption linewidth of the $\nu_2 + \nu_4$ combination band. There are small discrepancies in the background that may reflect inadequacies in the index of refraction and absorption corrections, but the DOVE features are well described by the model.

The Raman resonant $\chi^{(3)}$ of benzene has been measured to be 1.6×10^{-13} cm^3/erg for a two laser experiment with $2\omega_1 - \omega_2 = 19\,050$ cm^{-1} [12]. We assume that deuterobenzene has the same $\chi^{(3)}$ since its electronic states are not expected to be appreciably perturbed by the deuteration. The value must be corrected for the three laser frequencies used in this experiment using estimates described elsewhere [15]. The measured value of the DOVE-IRFWM $\chi^{(3)}$ is then 3.1×10^{-14} cm^3/erg, almost half the corrected value of the deuterobenzene CARS $\chi^{(3)}$ and 18 times larger than the acetonitrile nonresonant electronic background [see Table I].

We can also calculate the $\chi^{(3)}$ value because the factors for acetonitrile DOVE-IRFWM in Eq. (4) appear in the infrared absorption coefficients for the transitions to ν_2 and $\nu_2 + \nu_4$ and the Raman cross section for a transition involving ν_4 [16]. We assume that although the DOVE-IRFWM process requires a Raman transition between ν_2 and $\nu_2 + \nu_4$, we can use the data for the Raman transition from the ground state to ν_4 since the excitation of ν_2 should not change the electronic states appreciably. We use the value for the Raman resonant $\chi^{(3)}$, the molar absorptivities of acetonitrile, and the other values from Table I. The estimate again requires corrections for the differences in the frequencies used for the Raman measurement and the DOVE-IRFWM measurement. The calculated value of 2.7×10^{-14} cm^3/erg for the DOVE $\chi^{(3)}$ is within 15% of the measured value.

This work represents the first measurement of doubly vibrationally resonant FWM, and it shows that the enhancements are multiplicative and sufficiently large that multiresonant vibrational spectroscopy is feasible.

TABLE I. Parameter values required for calculating DOVE $\chi^{(3)}$ and values in the fitting routine to obtain experimental values for $\chi^{(3)}$. The 944 cm^{-1} deuterobenzene $\chi^{(3)}$ is the standard and relative uncertainties on the measurements are ±20%.

Literature	N (cm^{-3})	F	ε_{ba}, ε_{ca} (liter mole^{-1} cm^{-1})	Γ_{ba} (cm^{-1})	Γ_{ca} (cm^{-1})	Predicted $\chi^{(3)}$ (cm^3/erg)
CH_3CN	1.97×10^{22}	2.59	42.9, 3.16[a]	2.85[b]	4.39[c]	2.7×10^{-14}
C_6D_6	6.73×10^{21}	4.04		1.15[d]		7.1×10^{-14}
Experimental	CH_3CN DOVE	CH_3CN Raman[c]	CH_3CN NR[c]	C_6D_6 Raman[d]	C_6D_6 NR[d]	Windows[c]
A[c,e]			0.013		0.04	0.012
B/Γ_{ba}[c,e]		0.043		1		
$C/\Gamma_{ba}\Gamma_{ca}$[c,e]	0.232					
$D/\Gamma_{ba}\Gamma_{ca}$[c,e]	0.03					
Γ_{ba} (cm^{-1})	2.85[b]	2.72[c]		3.01[c]		
Γ_{ca} (cm^{-1})[c]	4.39					
ω_{ba} (cm^{-1})[c]	2253	918		944		
ω_{ca} (cm^{-1})[c]	3164					
$\chi^{(3)}$ expt[c] (cm^3/erg)	3.1×10^{-14}	5.75×10^{-15}	1.7×10^{-15}	7.1×10^{-14}[f]	2.8×10^{-15}[f]	1.6×10^{-15}

[a]Ref. [14]; [b]Ref. [25]; [c]This work; [d]Ref. [12]; [e]Peak values are normalized to the 944 cm^{-1} deuterobenzene hyperpolarizability.
[f]Published value was corrected for the frequencies used in this experiment [15].

Although this work used frequency domain methods, the same spectroscopy can be performed in the time domain [7]. There has been a great deal of interest in multiply resonant time domain six wave mixing (SWM) methods because they use Raman transitions that can access the entire vibrational frequency range [1,4,17,18]. However, SWM can be masked by cascaded FWM processes [19,20]. The frequency domain FWM DOVE methods do not experience interferences from cascaded three wave mixing, which is unimportant in isotropic materials, but they have the same useful characteristics as SWM.

The added spectral dimension of a doubly resonant spectroscopy significantly increases the resolution that can be achieved in complex samples. In fact, DOVE-IRFWM should be capable of line narrowing the inhomogeneously broadened lines that are commonly found in biological samples [3]. This narrowing is equivalent to coherence refocusing in time domain methods [1]. DOVE methods are particularly attractive for investigating complex samples because spectral congestion can be greatly reduced, not only by the possible line narrowing but also by the elimination of uncoupled transitions. Multiresonant spectra should contain only features that involve intra- or intermolecular interactions so they should isolate the features that are of most interest in many applications. These are the same types of features that Hamm and co-workers observe using a femtosecond 2D correlation spectroscopy where the interactions appear as correlated changes in pump-probe and hole burning spectra as different infrared features are excited [21,22] or that traditional 2D correlation spectroscopies observe using external perturbations to cause correlated changes [23]. It may thus be possible to observe the coupling between the C═O and N—H functionalities that are induced by H-bonding interactions in proteins and other biological molecules. Finally, the observable vibrational enhancements are limited in our work by the fluctuations in the nonresonant background. Since ultrafast pulses allow temporal discrimination against the background [24], the higher peak intensities that are possible with ultrafast DOVE methods should provide low detection limits.

This work was supported by the National Science Foundation under Grant No. CHE-9916829.

[1] Y. Tanimura and S. Mukamel, J. Chem. Phys. **99**, 9496 (1993).
[2] A. Zilian *et al.*, J. Lumin. **60&61**, 655 (1994).
[3] J. C. Wright *et al.*, Appl. Spectrosc. **51**, 949 (1997).
[4] T. Steffen and K. Duppen, Phys. Rev. Lett. **76**, 1224 (1996).
[5] K. Tominaga *et al.*, J. Raman Spectrosc. **26**, 495 (1995).
[6] A. Tokmakoff and G. R. Fleming, J. Chem. Phys. **106**, 2569 (1997).
[7] M. Cho, K. Okumura, and Y. Tanimura, J. Chem. Phys. **108**, 1326 (1998).
[8] J. C. Wright *et al.*, Int. Rev. Phys. Chem. **10**, 349 (1991).
[9] S. Mukamel, *Principles of Nonlinear Optical Spectroscopy* (Oxford University Press, New York, 1995), 1st ed.
[10] K. Okumura and Y. Tanimura, J. Chem. Phys. **106**, 1687 (1997).
[11] V. Chernyak and S. Mukamel, J. Chem. Phys. **108**, 5812 (1998).
[12] M. D. Levenson and N. Bloembergen, J. Chem. Phys. **60**, 1323 (1974).
[13] M. J. Labuda and J. C. Wright, Phys. Rev. Lett. **79**, 2446 (1997).
[14] J. E. Bertie and Z. Lan, J. Phys. Chem. B **101**, 4111 (1997).
[15] M. J. LaBuda and J. C. Wright, J. Chem. Phys. **108**, 4112 (1998).
[16] R. J. Carlson and J. C. Wright, Appl. Spectrosc. **43**, 1195 (1989).
[17] K. Tominaga and K. Yoshihara, Phys. Rev. Lett. **74**, 3061 (1995).
[18] A. Tokmakoff *et al.*, Phys. Rev. Lett. **79**, 2702 (1997).
[19] J. E. Ivanecky and J. C. Wright, Chem. Phys. Lett. **206**, 437 (1993).
[20] D. A. Blank, L. J. Kaufman, and G. R. Fleming, J. Chem. Phys. (to be published).
[21] P. Hamm, M. Lim, and R. M. Hochstrasser, J. Phys. Chem. B **102**, 6123 (1998).
[22] P. Hamm *et al.*, Proc. Natl. Acad. Sci. U.S.A. **96**, 2036 (1999).
[23] I. Noda, Appl. Spectrosc. **47**, 1329 (1993).
[24] K. D. Rector, D. Zimdars, and M. D. Fayer, J. Chem. Phys. **109**, 5455 (1998).
[25] S. Hashimoto, T. Ohba, and S. Ikawa, Chem. Phys. **138**, 63 (1989).